



Predicting diffused-bubble oxygen transfer rate using the discrete-bubble model

Daniel F. McGinnis, John C. Little*

Department of Civil and Environmental Engineering, Virginia Polytechnic Institute and State University, Blacksburg, VA 24061-0246, USA

Abstract

A discrete-bubble model that predicts the rate of oxygen transfer in diffused-bubble systems is evaluated. Key inputs are the applied gas flow rate and the initial bubble size distribution. The model accounts for changes in the volume of individual bubbles due to transfer of oxygen and nitrogen (and hence changing partial pressure), variation in hydrostatic pressure, and changes in temperature. The bubble-rise velocity and mass-transfer coefficient, both known functions of the bubble diameter, are continually adjusted. The model is applied to predict the results of diffused-bubble oxygen transfer tests conducted in a 14-m deep tank at three air flow rates. All of the test data are predicted to within 15%. The range of bubble diameters (0.2–2 mm) spans the region of greatest variation in rise velocity and mass-transfer coefficient. For simplicity, the Sauter-mean diameter is used rather than the full bubble size distribution without loss of accuracy. The model should prove useful in the design and optimization of hypolimnetic oxygenation systems, as well as other diffused-bubble applications. © 2002 Elsevier Science Ltd. All rights reserved.

Keywords: Aeration; Diffuser; Distribution; Mass transfer; Rise velocity

1. Introduction

Thermal stratification of reservoirs may result in substantial hypolimnetic oxygen depletion. Low dissolved oxygen (DO) levels have a negative impact on cold-water fisheries, hydropower discharges, and the drinking-water treatment process. In water-supply reservoirs, low DO may lead to the production of hydrogen sulfide and ammonia and can cause the release of soluble reduced iron and manganese from the sediments. Iron, manganese, and hydrogen sulfide impart undesirable color, taste, and odor to the water requiring additional treatment prior to distribution [1]. The increased oxidant demand at the water treatment plant increases costs and, if organic matter is present, may increase the concentration of disinfection byproducts.

In the case of hydropower reservoirs, the US Federal Energy Regulatory Commission typically requires that

releases meet local in-stream water-quality standards [2] with minimum DO levels of about 5 gm^{-3} . As a consequence, hydropower operators must frequently add large quantities of oxygen to stored water prior to or during discharge. For example, the Tennessee Valley Authority (TVA) spends about \$2M annually on liquid oxygen that is added to several of their hydropower reservoirs [3]. Hypolimnetic oxygenation has also been proposed by the US Army Corps of Engineers to replace fish habitat [4], creating an environment upstream of a hydropower dam that is preferred by cold-water species.

Hypolimnetic oxygenation is used to replenish DO in reservoirs while preserving stratification. Well-designed hypolimnetic oxygenators provide measurable increases in DO levels [5], decrease total iron, manganese, and hydrogen sulfide concentrations [6,7], and decrease blue-green algae concentrations in some cases [8,9]. Three principle devices are typically used for hypolimnetic oxygenation: the Speece Cone [10,11], the airlift aerator [12–15], and the bubble plume [16]. Typically, pure

*Corresponding author.

| Nomenclature | | | |
|--------------|--|----------------------|--|
| A | surface area, m^2 | v | velocity, m s^{-1} |
| C | aqueous-phase concentration, mol m^{-3} | V | volume, m^3 |
| C_D | drag coefficient, dimensionless | Y | gas-phase mole fraction, dimensionless |
| d | bubble diameter, m, mm | z | depth, m |
| D | diffusion coefficient, $\text{m}^2 \text{s}^{-1}$ | <i>Greek letters</i> | |
| g | gravitational constant, m s^{-2} | μ | viscosity, $\text{kg m}^{-1} \text{s}^{-1}$ |
| H | Henry's constant, $\text{mol m}^{-3} \text{bar}^{-1}$ | ρ | density, kg m^{-3} |
| J | mass-transfer flux, $\text{mol m}^{-2} \text{s}^{-1}$ | σ | interfacial surface tension, N m^{-1} |
| K_L | liquid-side mass-transfer coefficient, m s^{-1} | <i>Subscripts</i> | |
| m | mass, mol | 0 | initial |
| M | mass flux, mol s^{-1} | 3, 2 | Sauter-mean |
| n | number of bubbles | b | bubble |
| N | number flux of bubbles, s^{-1} | d | diffuser |
| P | pressure, bar | G | gas |
| q | gas flow rate per unit length, $\text{m}^2 \text{s}^{-1}$ | i | individual, partial |
| Q | volumetric flow rate, $\text{m}^3 \text{s}^{-1}$ | L | liquid |
| r | bubble radius, m | s | saturated |
| R | ideal gas constant, $\text{m}^3 \text{bar mol}^{-1} \text{K}^{-1}$ | std | standard |
| Re | Reynolds number, dimensionless | x | horizontal |
| Sc | Schmidt number, dimensionless | z | vertical |
| t | time, s | | |
| T | temperature, $^{\circ}\text{C}$, K | | |

oxygen is used in the Speece Cone, air is used in airlift aerators, and either oxygen or air is used in bubble plumes.

In all three oxygenation devices, gas bubbles in contact with water facilitate interfacial transfer of oxygen, as well as nitrogen and other soluble gases. Bubble size is a critical parameter in these diffused-bubble systems because it determines the interfacial surface area, bubble-rise velocity, and mass-transfer coefficient [17]. In addition, bubble size may vary significantly as the bubbles pass through the system, especially when pure oxygen is used. For these reasons, Wüest et al. [16] used a discrete-bubble model to account for changes in the volume (due to gas transfer, hydrostatic pressure, and water temperature) of individual bubbles rising within a bubble plume. This approach has subsequently been applied to airlift aerators [13,18], the Speece Cone [10], and a bubble plume [19,20]. Although limited versions of this approach have been used in diffused-bubble wastewater and ozonation systems [21–23], the discrete-bubble model has yet to be independently verified.

In this paper, the discrete-bubble model is used to predict the rate of oxygen transfer during diffused-bubble aeration, based solely on knowledge of the initial bubble-size distribution and the applied air flow rate. In addition, it is shown that the Sauter-mean diameter [24] may be used instead of a bubble size distribution without any loss of computational accuracy.

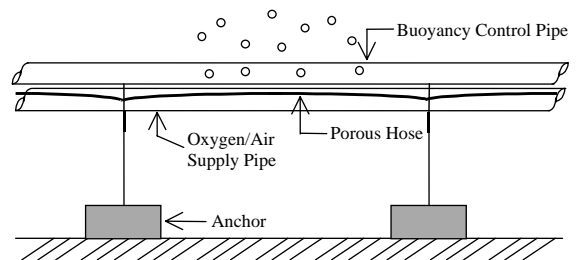


Fig. 1. Schematic of TVA's porous "soaker" hose diffuser.

2. Experimental methods

2.1. Oxygen transfer tests

Oxygen transfer tests were conducted in a 14-m high \times 2-m diameter tank with a porous "soaker" hose diffuser [2] used to generate bubble-plumes. A schematic representation of the diffuser arrangement is shown in Fig. 1. A 1.5-m length of diffuser with 2×1.5 -m lengths of 6.4-mm diameter porous hose was located 0.6 m above the base of the tank. DO in the water was removed using sodium sulfite with cobalt chloride as a catalyst. Tests were performed at air flow rates of 0.43, 0.68, and $2.88 \text{ N m}^3 \text{ h}^{-1}$, where 1 N m^3 denotes 1 m^3 of gas at 1 bar and 0°C . The air flow rate was measured

using a calibrated rotameter. The temperature of the water remained constant at 23°C during the tests. DO was measured using probes placed in the tank at depths of 3, 8, and 12 m below the water surface.

2.2. Measurement and representation of bubble-size distribution

In a separate series of experiments, a single 30-cm length of porous hose was placed 50 cm above the base of the tank, and positioned 9 cm behind a glass porthole along with a graduated scale (2-mm resolution). Tests were conducted at four air flow rates and at water depths of 6.7 and 12.5 m to determine the effect of air flow rate and hydrostatic pressure on initial bubble size. Duplicate tests were performed at approximately the same air flow rates and water depth. As shown in Fig. 2, photographs of the bubble swarm immediately above the porous hose were taken through the porthole.

The photographs were digitized and 20 bubbles were randomly selected for measurement. Previous research suggests that a total of 20 bubbles will provide a representative sample [25–27]. Because the larger bubbles are typically not perfectly spherical, the horizontal

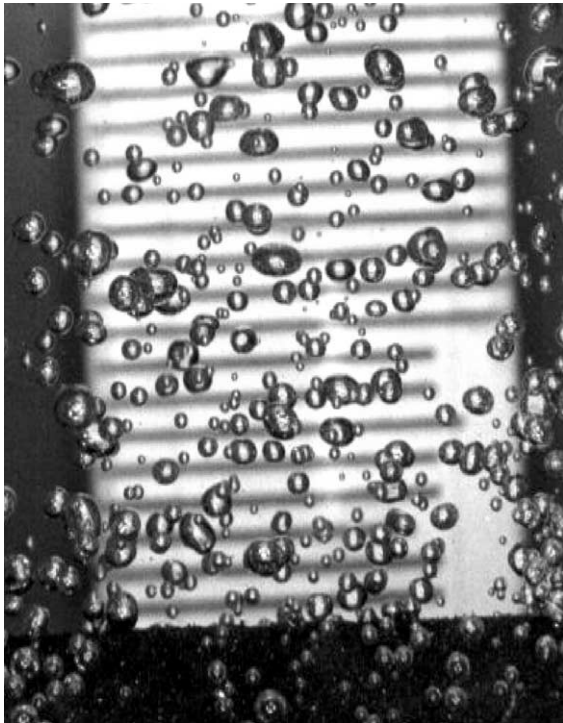


Fig. 2. Photograph of bubbles formed by a porous diffuser at a water depth of 12.5 m. The actual air flow rate per unit length for this 30-cm section was $q = 0.83 \text{ m}^2 \text{ h}^{-1}$ yielding a Sauter-mean bubble diameter of 1.9 mm.

and vertical axis of each bubble was measured. The surface area of a bubble, A , is

$$A = \pi d_x d_z (\text{mm}^2), \quad (1)$$

where d_x and d_z are the bubble diameters in the horizontal and vertical axis, respectively. The equivalent spherical diameter is

$$d = \sqrt{\frac{A}{\pi}} (\text{mm}). \quad (2)$$

Because of the increased complexity of applying the discrete-bubble model using the entire bubble size distribution, a Sauter-mean diameter was calculated for each distribution. The Sauter-mean diameter is the diameter of a sphere having the same volume-to-surface ratio as the distribution of bubbles [28,24], or

$$d_{3,2} = \frac{\sum_{i=1}^n d_i^3}{\sum_{i=1}^n d_i^2} (\text{mm}), \quad (3)$$

where d_i is the diameter of the individual bubbles and n is the number of bubbles in the sample. This formula gives more weight to larger bubbles, and is therefore more representative for mass transfer than the mean bubble diameter [24].

3. Discrete-bubble model

The discrete-bubble model, first adopted by Wüest et al. [16], is applied to bubbles that rise in plug flow through a tank of well-mixed water. The initial bubble size distribution and the rate of bubble formation are assumed to be constant. Bubble coalescence and mass transfer of gases other than nitrogen and oxygen are considered negligible. The water and air temperatures are assumed to be equal and constant. Mass transfer through the water surface at the top of the tank is neglected. Finally, it is assumed that a distribution of bubble sizes may be represented by the Sauter-mean diameter.

The mass-transfer flux (for either oxygen or nitrogen) across the surface of a bubble is

$$J = K_L(C_s - C) (\text{mol m}^{-2} \text{ s}^{-1}), \quad (4)$$

where K_L is the liquid-side mass-transfer coefficient, C_s is the equilibrium concentration at the gas/water interface, and C is the bulk aqueous-phase concentration. For both oxygen and nitrogen, gas-side mass-transfer resistance may be neglected. Henry's law is used to calculate the equilibrium concentration, or

$$C_s = HP_i (\text{mol m}^{-3}), \quad (5)$$

where H is Henry's constant and P_i is the partial pressure of the gas at a given depth. Combining Eqs. (4) and (5) yields

$$J = K_L(HP_i - C) (\text{mol m}^{-2} \text{ s}^{-1}). \quad (6)$$

Table 1

Correlation equations for Henry’s constant ($\text{mol m}^{-3} \text{bar}^{-1}$), mass transfer coefficient (m s^{-1}), and bubble-rise velocity (m s^{-1}) [16]

| Correlation equation | Range |
|--|---|
| $H_{\text{O}} = 2.125 - 5.021 \times 10^{-2}T + 5.77 \times 10^{-4}T^2$ (T in $^{\circ}\text{C}$) | |
| $H_{\text{N}} = 1.042 - 2.450 \times 10^{-2}T + 3.171 \times 10^{-4}T^2$ (T in $^{\circ}\text{C}$) | |
| $K_{\text{L}} = 0.6r$ $K_{\text{L}} = 4 \times 10^{-4}$ | $r < 6.67 \times 10^{-4} \text{ m}$ $r \geq 6.67 \times 10^{-4} \text{ m}$ |
| $v_{\text{b}} = 4474r^{1.357}$ $v_{\text{b}} = 0.23$ $v_{\text{b}} = 4.202r^{0.547}$ | $r < 7 \times 10^{-4} \text{ m}$ $7 \times 10^{-4} \leq r < 5.1 \times 10^{-3} \text{ m}$ $r \geq 5.1 \times 10^{-3} \text{ m}$ |

Substituting the surface area of a bubble of radius r gives the rate of mass transfer for a single bubble as

$$\frac{dm}{dt} = -K_{\text{L}}(HP_i - C)4\pi r^2 \text{ (mol s}^{-1}\text{)}. \tag{7}$$

The vertical location of the bubble is related to the bubble-rise velocity, v_{b} , and any induced vertical water velocity, v , by

$$\frac{dz}{dt} = v + v_{\text{b}} \text{ (m s}^{-1}\text{)}, \tag{8}$$

where z is the vertical coordinate of the tank. Although the bulk of the water in the tank is assumed to be well-mixed, it is likely that a weak plume is formed immediately above the diffuser in the core of the tank. For simplicity, it is assumed that the induced plume velocity is low relative to the bubble-rise velocity. Combining Eqs. (7) and (8) gives the mass of gaseous species transferred per bubble per unit height of tank

$$\frac{dm}{dz} = -K_{\text{L}}(HP_i - C)\frac{4\pi r^2}{v_{\text{b}}} \text{ (mol m}^{-1}\text{)}. \tag{9}$$

The number flux of bubbles entering the tank, N , is calculated from the initial bubble volume, V_0 , and the actual volumetric gas flow rate at the diffuser, Q_0 , or

$$N = \frac{Q_0}{V_0} \text{ (s}^{-1}\text{)}. \tag{10}$$

Multiplying Eq. (9) by N and expressing it in terms of M , the molar flow rate of gas, yields

$$\frac{dM}{dz} = -K_{\text{L}}(HP_i - C)\frac{4\pi r^2 N}{v_{\text{b}}} \text{ (mol m}^{-1} \text{ s}^{-1}\text{)}. \tag{11}$$

If the bulk aqueous-phase concentration does not change significantly during the time a bubble takes to rise through the tank, the pseudo-steady-state assumption may be invoked. Eq. (11) is integrated numerically, for both oxygen and nitrogen, to obtain the change in the molar flow rate while the gas bubble is in contact with the water. H is a function of water temperature, while v_{b} and K_{L} are functions of r , the radius of the bubble. The bubble radius changes in response to decreasing hydrostatic pressure as well as the amount

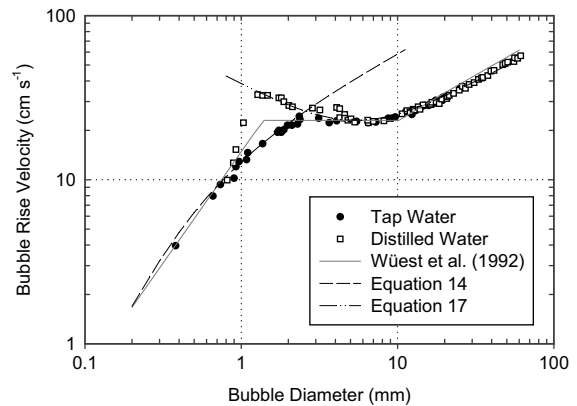


Fig. 3. Bubble-rise velocity as a function of bubble diameter. Data from Haberman and Morton [31].

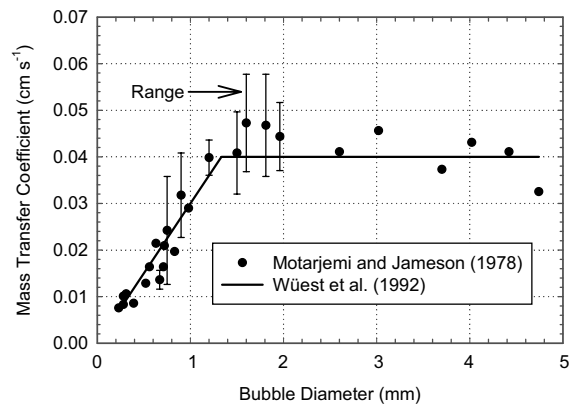


Fig. 4. Liquid-side mass-transfer coefficient for individual bubbles as a function of bubble diameter. Data from Motarjemi and Jameson [17].

of oxygen and nitrogen transferred between the bubble and the water. This results in a change in the partial pressure of oxygen and nitrogen within the bubble, which is recalculated as the bubble rises through the tank. As summarized in Table 1, relationships for v_{b}

(Fig. 3) and K_L (Fig. 4) were developed by Wüest et al. [16] based on experimental data for bubble-rise velocity [31] and the mass-transfer coefficient [17]. Using these relationships and the changing bubble radius, both the bubble-rise velocity and the mass-transfer coefficient are recalculated as the bubble travels up the tank. Once the bubble reaches the top of the tank, the overall change in the molar flow rate of gas (both oxygen and nitrogen) is used to incrementally calculate the evolving bulk aqueous-phase concentration as a function of time.

The initial DO concentration, water temperature, and depth are known, as well as the initial Sauter-mean diameter of the bubble swarm formed at the diffuser. The initial dissolved nitrogen concentration is assumed to be at equilibrium with the atmosphere. The initial molar flow rate of gaseous oxygen or nitrogen is

$$M_0 = \frac{Y_0 P_{\text{std}} Q_{\text{std}}}{RT_{\text{std}}} \quad (\text{mol s}^{-1}), \quad (12)$$

where Y_0 is the initial mole fraction of the gas, P_{std} is the standard pressure, Q_{std} is the gas flow rate at standard temperature and pressure (0°C and 1 bar), R is the ideal gas constant, and T_{std} is the standard temperature.

4. Results and discussion

The results of the three oxygen transfer tests are shown in Fig. 5. For each of the tests, the response of the three oxygen probes (located near the top, middle, and bottom of the tank) was virtually identical, confirming that the water in the tank can be considered well-mixed. Because the data obtained from the three probes were almost equal, the three data sets were averaged to obtain one representative oxygen concentration profile for each experiment. To apply the discrete-bubble model, the

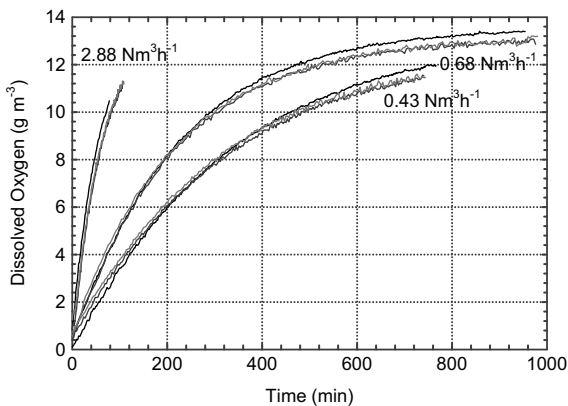


Fig. 5. Mass-transfer test results showing measured DO concentrations as a function of time. Data were collected using three oxygen probes located at depths of 3, 8, and 12 m.

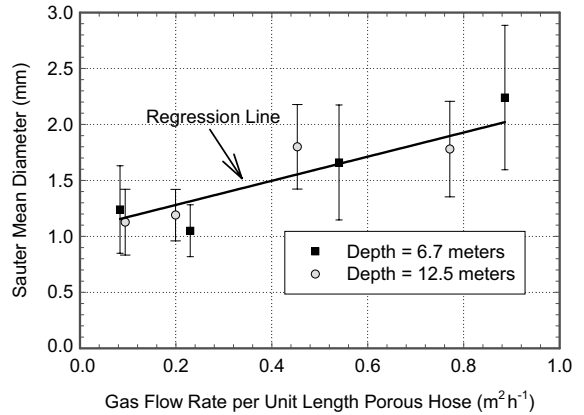


Fig. 6. Initial bubble size formed by porous hose as a function of gas flow rate and water depth. Bars represent 1 standard deviation.

initial bubble size for each of the air flow rates is required.

Fig. 6 summarizes the results of the bubble size measurements. The measured initial Sauter-mean diameter is shown as a function of the actual volumetric gas flow rate for the tests performed at depths of 6.7 and 12.5 m. Since there was essentially no difference between the bubble sizes formed at these two different depths, a simple linear relationship was developed relating bubble size to gas flow rate:

$$d_{3,2} = 1.12 + 0.938q \quad (\text{mm}), \quad (13)$$

where q is the actual gas flow rate per unit length of porous hose in units of $\text{m}^2 \text{h}^{-1}$. Eq. (13), which was derived from data collected using a 30-cm length of porous hose, was then used to predict the initial bubble size for each of the three diffuser experiments. The Sauter-mean diameters obtained were 1.2, 1.2, and 1.6 mm for the 0.43, 0.68 and $2.88 \text{ Nm}^3 \text{ h}^{-1}$ tests, respectively. These bubble sizes and the measured air flow rates were used as input to the discrete-bubble model to predict the oxygen concentration as a function of time. The predicted results are compared in Fig. 7 to the average of the values measured with the three oxygen probes. The observed and predicted DO curves compare well, with root mean square errors of 0.65, 0.60 and 1.31 for the 0.43, 0.68 and $2.88 \text{ Nm}^3 \text{ h}^{-1}$ tests, respectively. The initial predicted oxygen transfer efficiency ranges from 94.4% at the lowest air flow rate to 88.1% at the highest air flow rate. Although the model tends to overestimate the oxygen concentrations, nearly all of the predictions fall within 15% of the observed data, as shown in Fig. 8. As indicated in Fig. 6, the independently measured initial bubble sizes had a relatively high degree of variability. Given that the model is sensitive to the initial bubble size, it may be that the bubble-size

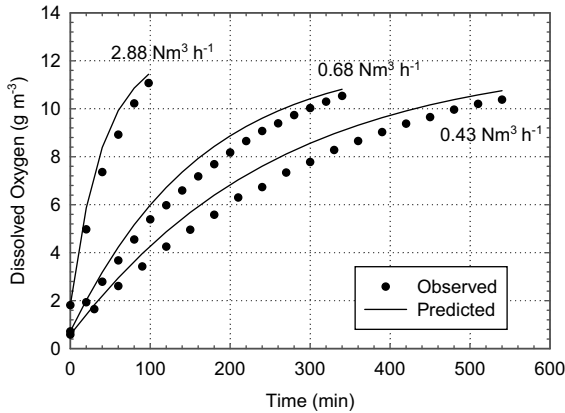


Fig. 7. Average observed DO concentrations versus those predicted using the discrete-bubble model.

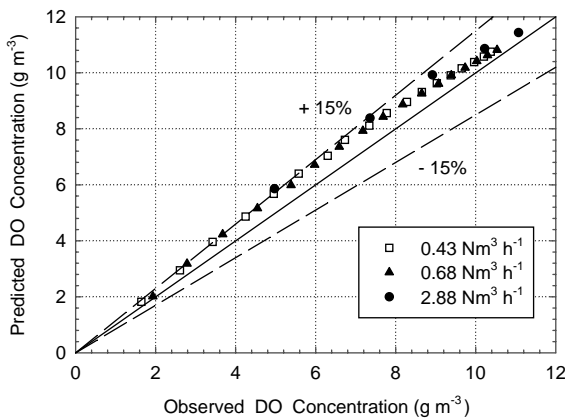


Fig. 8. Predicted versus observed DO concentrations.

estimation procedure is the primary source of the modest error. In the following sections, some of the key assumptions and limitations of the discrete-bubble model are briefly evaluated.

4.1. Bubble-size distribution

The Sauter-mean diameter may not accurately represent the average bubble-rise velocity or mass-transfer coefficient of the bubble swarm. Smaller bubbles, in particular, have rise velocities and mass-transfer coefficients that are very sensitive to bubble diameter. To check the validity of the Sauter-mean diameter, the discrete-bubble model was modified to accommodate a range of bubble sizes. The bubble size distribution for the $0.68 \text{ Nm}^3 \text{ h}^{-1}$ oxygen transfer test was obtained from the bubble size data measured at $0.09 \text{ m}^2 \text{ h}^{-1}$ because the actual flow rates (i.e., measured at the diffuser depth) per unit length of porous hose were

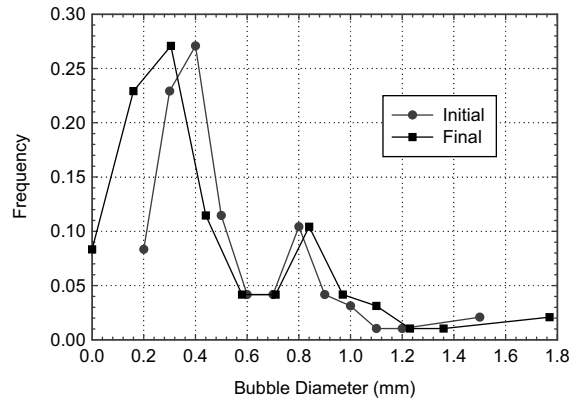


Fig. 9. Initial (measured) and final (predicted) bubble size distribution, based on the oxygen transfer experiment conducted at an air flow rate of $0.68 \text{ Nm}^3 \text{ h}^{-1}$.

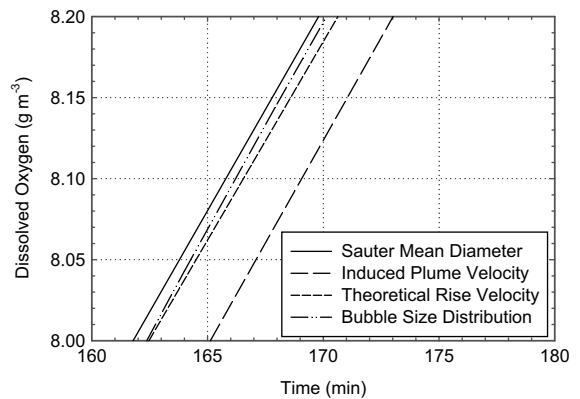


Fig. 10. Comparison of discrete-bubble model predictions based on Sauter-mean diameter to those obtained by introducing an induced plume velocity, using the theoretical bubble-rise velocity, and using a bubble size distribution.

approximately equal. As shown in Fig. 9, the initial bubble diameters in this distribution vary from 0.2 to 1.5 mm and span the range of rapid variation in bubble-rise velocity and mass-transfer coefficient. Fig. 9 also shows the final bubble size distribution predicted for the bubbles at the top of the tank. Using the entire bubble size distribution instead of the Sauter-mean diameter produced a similar rate of oxygen transfer, as shown in Fig. 10.

4.2. Bubble-rise velocity

The discrete-bubble model uses correlation equations to determine terminal rise velocity based on data collected by Haberman and Morton [31]. As shown in Fig. 3, for diameters between 1 and 2 mm, the bubble-

rise velocities in distilled and tap water are quite different, with the Wüest et al. [16] correlation falling between the two data sets. Since bubbles in tap water smaller than about 2 mm behave as rigid spheres with regard to rise velocity [31], the terminal rise velocity can be calculated from

$$v_b = \left[\frac{4d_b g (1 - \rho_G / \rho_L)}{3C_D} \right]^{1/2}, \quad (14)$$

where ρ_G and ρ_L are the densities of the gas and liquid, respectively. C_D is the drag coefficient, expressed as

$$C_D = \frac{24}{Re} + \frac{3}{\sqrt{Re}} + 0.34, \quad (15)$$

where Re , the Reynolds number, is

$$Re = \frac{v_b d_b \rho_L}{\mu_L} \quad (16)$$

and μ_L is the dynamic viscosity of water. Fig. 3 shows that Eq. (14) predicts the tap water data up to a bubble diameter of 2.6 mm.

Larger bubbles begin to experience surface oscillations and the rise of the bubble can be compared to a wave traveling in an ideal fluid [29]. Based on this wave analogy, the rise velocity of larger bubbles can be predicted [29] by

$$v_b = \sqrt{\frac{2\sigma}{d_b(\rho_L + \rho_G)} + \frac{gd_b}{2}}, \quad (17)$$

where σ is the interfacial surface tension of water. Fig. 3 shows that Eq. (17) can be used to predict the rise velocity for bubbles larger than 2.6 mm in tap water. Since the tap water data appear more appropriate for hypolimnetic oxygenation, Eqs. (14) and (17) can be used to predict the theoretical rise velocity for the entire range of bubble sizes and have the added benefit of including the dependence on temperature. However, using the theoretical rise velocity instead of the Wüest et al. [16] correlation made essentially no difference to the model predictions, with values shown for comparative purposes in Fig. 10.

4.3. Mass-transfer coefficient

The mass-transfer coefficient is also estimated using a correlation equation developed by Wüest et al. [16]. The correlation shown in Fig. 4 gives the mass-transfer coefficient for oxygen and nitrogen as a function of bubble radius for bubbles of diameter less than approximately 1.3 mm, and assumes a constant mass-transfer coefficient for bubbles larger than 1.3 mm in diameter. Unfortunately, the data in Fig. 4 were not referenced to a specific water temperature [17] and could not be corrected to the temperature of the oxygen transfer tests (23°C). The temperature dependence of

the mass-transfer coefficient is given [30] by

$$K_L(T^\circ\text{C}) = K_L(20^\circ\text{C}) \left[\frac{Sc(20^\circ\text{C})}{Sc(T^\circ\text{C})} \right]^{1/2}, \quad (18)$$

where

$$Sc = \frac{\mu_L}{\rho_L D_L} \quad (19)$$

is the Schmidt number and D_L is the diffusion coefficient of oxygen or nitrogen in water. Assuming the data of Motarjemi and Jameson [17] were collected at 20°C, the mass-transfer coefficients for both oxygen and nitrogen would increase by about 8% because the experiments were conducted at 23°C. However, this correction makes very little difference to the predicted oxygen concentration profiles shown in Fig. 7 because the oxygen transfer process is approaching saturation. This holds at the beginning of the experiment when the oxygen transfer efficiency is high, as well as towards the end of the experiment when the aqueous concentration approaches steady state.

4.4. Induced water velocity

Another assumption made during the application of the model is that any induced water velocity is negligible. If this assumption is not correct, then the water velocity would decrease the bubble contact time and reduce the extent to which the model over-predicts the experimental data. Efforts were made to measure the induced water velocity, but it was found to be less than 0.04 m s^{-1} , the lower measurement limit of the velocity meter used. The discrete-bubble model was modified to include a uniform vertical velocity (see Eq. (8)) equal to 0.04 m s^{-1} , but Fig. 10 shows that this results in only a modest decrease in the predicted oxygen concentrations.

5. Conclusion

The predictions of the discrete-bubble model were compared to the results of diffused-bubble oxygen transfer tests conducted in a 14-m deep tank at three air flow rates. Required model inputs are the gas flow rate and the initial bubble size distribution. Although the bubble-size distribution can be taken into account, using the Sauter-mean diameter is simpler and provides equivalent results. Based on correlation equations for bubble-rise velocity and the mass-transfer coefficient developed by Wüest et al. [16], the model predicts all the oxygen transfer test data to within 15%. The range of bubble diameters measured during the tests was from 0.2 to 2 mm, spanning the region of greatest variation in rise velocity and mass-transfer coefficient. The discrete-bubble model has also been applied to predict oxygen transfer in a full-scale airlift aerator [18], where the

range of bubble diameters was from about 2 to 4 mm. Although the model tends to over-estimate the rate of oxygen transfer in the well-mixed tank and under-estimate the rate in the airlift aerator, the combined results suggest that the model is reliable for bubble sizes between 0.2 and 4 mm. In both cases, the initial bubble sizes were measured in laboratory experiments carried out completely independent of the oxygen transfer tests. Since both sets of data had a relatively high degree of variability and because the model is sensitive to initial bubble size, it appears plausible that the bubble-size estimation procedure is the primary source of the modest error.

The discrete-bubble model has been successfully used to predict oxygen transfer in a well-mixed tank (this work), an airlift aerator [18], and a bubble plume [19,20]. The discrete-bubble approach has also been applied to the Speece Cone [10], but the model could not be fully verified due to a lack of experimental data. Because it is known that hypolimnetic oxygenators can induce varying degrees of mixing in a stratified reservoir [19], the suite of models is being coupled with a hydrodynamic and water-quality reservoir model so that oxygenation systems can be designed more effectively and operated more efficiently.

Acknowledgements

Financial support was provided by the National Science Foundation (NSF) through an NSF CAREER Award (Grant No. 9624488) with supplemental funding from the Tennessee Valley Authority and Roanoke County, Virginia. Special thanks are extended to Vickie Burris for her assistance with the experimental work.

References

- [1] Cooke GD, Carlson RE. Reservoir management for water quality and THM precursor control. AWWA Research Foundation, Denver, CO, 1989. 387pp.
- [2] Mobley MH. TVA reservoir aeration diffuser system, TVA Technical Paper 97-3. ASCE Waterpower '97, Atlanta, GA, August 5–8, 1997.
- [3] Hauser GE. Personal communication. TVA Engineering Lab, 129 Pine Rd, Norris, TN 37828, 2000.
- [4] United States Army Corps of Engineers. 3.7.2 habitat replacement system. From the Draft Environmental Assessment and Finding of No Significant Impact, R. B. Russell Dam and Lake Project Pumped Storage, November 1998.
- [5] Gächter R. Ten years experience with artificial mixing and oxygenation of prealpine lakes. *Lake Reserv Manage* 1995;11:141.
- [6] McQueen DJ, Lean DRS. Hypolimnetic aeration: an overview. *Water Pollut Res J Can* 1986;21:205–17.
- [7] Thomas JA, Funk WH, Moore BC, Budd WW. Short term changes in Newman Lake following hypolimnetic aeration with Speece Cone. *Lake Reserv Manage* 1994;9:111–3.
- [8] Gemza A. Some practical aspects of whole lake mixing and hypolimnetic oxygenation. Ecological impacts of aeration on lakes and reservoirs in southern Ontario. *Lake Reserv Manage* 1995;11:141.
- [9] Kortmann RW, Knoecklein GW, Bonnell CH. Aeration of stratified lakes: theory and practice. *Lake Reserv Manage* 1994;8:99–120.
- [10] McGinnis DF, Little JC. Bubble dynamics and oxygen transfer in a Speece Cone. *Water Sci Technol* 1998; 37(2):285–92.
- [11] Speece RE, Rayyan F, Murfee G. Alternative considerations in the oxygenation of reservoir discharges and rivers. In: Speece RE, Malina Jr JF, editors. Applications of commercial oxygen to water and wastewater systems. Austin, TX: Center for Research in Water Resources, 1973. p. 342–61.
- [12] Ashley KI. Hypolimnetic aeration: practical design and application. *Water Res* 1985;19:735–40.
- [13] Burris VL, Little JC. Bubble dynamics and oxygen transfer in a hypolimnetic aerator. *Water Sci Technol* 1998; 37(2):293–300.
- [14] Fast AW, Dorr VA, Rosen RJ. A submerged hypolimnion aerator. *Water Resour Res* 1975;11:287–93.
- [15] Little JC. Hypolimnetic aerators: predicting oxygen transfer and hydrodynamics. *Water Res* 1995;29:2475–82.
- [16] Wüest A, Brooks NH, Imboden DM. Bubble plume modeling for lake restoration. *Water Resour Res* 1992; 28:3235–50.
- [17] Motarjemi M, Jameson GJ. Mass transfer from very small bubbles—the optimum bubble size for aeration. *Chem Eng Sci* 1978;33:1415–23.
- [18] Burris VL, McGinnis DF, Little JC. Predicting oxygen transfer and water flow rate in airlift aerators. *Water Res*, 2002 this issue.
- [19] Little JC, McGinnis DF. Hypolimnetic oxygenation: predicting performance using a discrete-bubble model. *Water Sci Technol: Water Supply* 2001;1(4):185–91.
- [20] McGinnis DF, Little JC, Wüest A. Hypolimnetic oxygenation: coupling bubble-plume and reservoir models. Proceedings of Asian WATERQUAL, IWA Regional Conference, Fukuoka, Japan, September 2001.
- [21] Bin AK. Application of a single-bubble model in estimation of ozone transfer efficiency in water. *Ozone Sci Eng* 1995;17:469–84.
- [22] Bischof F, Durst F, Hofken M, Sommerfeld M. Theoretical considerations about the development of efficient aeration systems for activated sludge treatment. *Aeration Technol: ASME* 187;1994:27–38.
- [23] Pöpel HJ, Wagner M. Prediction of oxygen transfer from simple measurements of bubble characteristics. *Water Sci Technol* 1991;23:1941–50.
- [24] Orsat V, Vigneault C, Raghavan GSV. Air diffusers characterization using a digitized image analysis system. *Appl Eng Agric* 1993;9:115–21.
- [25] Ashley KI, Hall KJ. Factors influencing oxygen transfer in hypolimnetic aeration systems. *Verh Int Verein Limnol* 1990;24:179–83.

- [26] Ashley KI, Hall KJ, Mavinic DS. Factors influencing oxygen transfer in fine pore diffused aeration. *Water Res* 1991;25:1479–86.
- [27] Chen S, Timmons MB, Aneshansley DJ, Bisogni Jr JJ. Bubble size distribution in a bubble column applied to aquaculture systems. *Aquaculture Eng* 1993;11:267–80.
- [28] Chisti MY. *Airlift bioreactors*. New York, NY: Elsevier Science Publishing, 1989. 345pp.
- [29] Jamialahmadi M, Branch C, Müller-Steinhagen H. Terminal bubble rise velocity in liquids. *Trans IChemE* 1994;2(Part A):119–22.
- [30] Daniil EI, Gulliver JS. Temperature dependence of liquid-film coefficient for gas transfer. *J Environ Eng* 1988; 114(5):1224–9.
- [31] Haberman WL, Morton RK. An experimental study of bubbles moving in liquids. *Proc Am Soc Civ Eng* 1954; 80:379–427.